Polymer Chemistry

PAPER

View Article Online
View Journal | View Issue

Cite this: *Polym. Chem.*, 2014, **5**, 6797

Synthesis and properties of D–A copolymers based on dithienopyrrole and benzothiadiazole with various numbers of thienyl units as spacers†

Yanfang Geng,[a] Junzi Cong,[b] Keisuke Tajima,*[b] Qingdao Zeng[a] and Erjun Zhou*[a]

Received 17th July 2014,
Accepted 14th August 2014

DOI: 10.1039/c4py00975d

www.rsc.org/polymers

Three kinds of donor–acceptor (D–A) type semiconducting copolymers in which electron donating units of dithienopyrrole (DTP) and accepting units of benzothiadiazole (BT) were connected with different numbers of thienyl spacers (x = 0–2) were synthesized and used as electron donor materials in polymer solar cells (PSCs) combined with fullerene derivatives. The optical band gaps of the polymers could be tuned from 1.41 eV to 1.61 eV by changing the number of thiophene spacers. Electrochemical measurements showed that the increase of band gap is mainly due to the change of the lowest unoccupied molecular orbital (LUMO) energy level. The power conversion efficiency (PCE) of the polymer solar cells based on the three polymers and $PC_{70}BM$ reached 3.12% with x = 2 under the illumination of AM 1.5, 100 mW cm^{-2}. This approach could provide a simple strategy for designing high-performance D–A type photovoltaic polymers based on the existing polymers and a large potential to improve their performance further.

1 Introduction

Polymer solar cells (PSCs) have attracted much interest due to their great potential to be a renewable energy technology based on simple and low cost manufacture.[1–3] The concept of a bulk heterojunction (BHJ) utilizing mixtures of a conjugated polymer and a fullerene derivative is regarded as an efficient system for photovoltaic application.[4] The most representative active layers of the blend of regioregular poly(3-hexylthiophene) (P3HT) with fullerene derivatives were extensively investigated.[5–7] While the advantage of P3HT is its simple structure with a relatively high hole mobility, the weak point of P3HT as the photovoltaic donor material towards efficient PSCs is the mismatch of its absorption spectrum (absorption edge is about 650 nm) with the terrestrial solar spectrum. The band gap of P3HT (1.9 eV) is larger than the optimum band gap range (1.3–1.5 eV) for polymer–fullerene BHJ solar cells.[8] Hence, design of photovoltaic polymers with broader absorption toward longer wavelengths, especially in the near-infrared (NIR) range, is necessary for high efficiency conjugated polymer donor materials.

Thanks to the many attempts that have been made to develop NIR absorbing polymers, a notable improvement of the overall power-conversion efficiency (PCE) has been achieved.[9–11] One of the most powerful and flexible strategies to design low band gap conjugated polymers involves an alternating sequence of electron-donor (D) and electron-acceptor (A) moieties along the conjugated polymer main chain.[12,13] The highest occupied molecular orbital (HOMO) and the lowest unoccupied molecular orbital (LUMO) of this so-called donor–acceptor (D–A) type copolymers are mainly localized on the donor and acceptor units, respectively, thus the band gap can be well tuned by the choice of D and A. Such a D–A strategy is now widely used as one of the most promising approaches to design efficient polymers for application to the polymer photovoltaic.

Thiophene is a simple and fundamental block to construct new D–A type copolymers. Recently, the bridged dithiophene has attracted considerable attention as a donor unit because of its ability to fix the dithiophene system into a planar structure, which is much more efficient than the dithiophene in constructing highly-conjugated copolymers. Four bridging dithiophene units with the atoms of carbon (C), silicon (Si), germanium (Ge) and nitrogen (N) afford cyclopenta[2,1-*b*;3,4-*b*′]-dithiophene (CPDT), dithienosilole (DTS), dithienogermole (DTG) and dithieno[3,2-*b*:2′,3′-*d*]pyrrole (DTP), respectively.

CPDT was first introduced into the low band gap polymers, and the corresponding copolymer alternating CPDT with benzothiadiazole showed a PCE of 5.5%, after using a small amount of alkanedithiols to control the morphology of the

[a]*National Center for Nanoscience and Technology, No. 11, Beiyitiao, Zhongguancun, Beijing 100190, P. R. China. E-mail: zhouej@nanoctr.cn*
[b]*Emergent Functional Polymers Research Team, RIKEN Center for Emergent Matter Science (CEMS), 2-1 Hirosawa, Wako 351-0198, Japan. E-mail: keisuke.tajima@riken.jp*

†Electronic supplementary information (ESI) available: XRD patterns, DFT and TD-DFT calculations. See DOI: 10.1039/c4py00975d

blend film.[14,15] Later on, large amounts of CPDT-based photovoltaic polymers were designed and synthesized.[16–20] In comparison with the C–C bond, a longer C–Si bond shows less steric hindrance, which directly resulted in better π–π stacking along the conjugated polymer backbones.[21,22] Polymers based on DTS normally have high hole mobility and strong light absorption in the visible region of the solar spectrum and hence the improvement in photovoltaic performance, which reached 5.1%.[12] DTG shows lower intermolecular steric hindrance than DTS because of the longer C–Ge bond compared to the C–Si, resulting in the corresponding DTG-containing solar cells exhibiting higher short-current and fill factor.[23–25] Planar dithieno[3,2-*b*:2′,3′-*d*]pyrrole (DTP), with good π-conjugation, showed great potential for use in organic electronic materials.[26] D–A type photovoltaic polymers with DTP as the electron-donating unit, exhibiting low band gap and enhanced solubility, have been intensively applied to PSCs.[27,28] In our previous study, PSCs based on DTP-containing copolymers and $PC_{70}BM$ showed a short-circuit current as high as 22.6 mA cm^{-1},[29] indicating that DTP-containing copolymers could be promising building blocks for superior photovoltaic performance.

On the other hand, benzothiadiazole (BT) containing the electron-withdrawing imine (–C═N–) nitrogen has been widely used as a strong acceptor in D–A copolymers.[30,31] Numerous attempts to develop novel D–A copolymers have shown that 4,7-dithien-2-yl-2,1,3-benzothiadiazole (DTBT) is an effective acceptor unit, and photovoltaic devices made from blends with fullerene derivatives show PCE up to 5.4%.[14,32–36] In 2008, we reported the synthesis of a copolymer between the DTP donor and the DTBT acceptor.[27] It has been proved that the thienyl ring can enhance the π–π stacking intermolecular interactions and lead to a high charge carrier mobility.[37] In addition, the ordered structure can enhance the carrier mobility; thereby symmetric thienyl units along the polymer main chain are selected. In this regard, a simple and effective method might be to tune the properties of D–A type photovoltaic polymers by introducing thienyl groups as spacers between donor and acceptor segments in the backbone.

In this study, three kinds of low band gap copolymers integrating DTP as the donor block and the most-used BT as the acceptor unit were synthesized. Different numbers of thienyl (T) as spacers were introduced along the copolymer main chain to investigate the effect on optical, electrochemical and photovoltaic performance. [6,6]-Phenyl-C_{71}-butyric acid methyl ester ($PC_{70}BM$) was used as an acceptor in the blended film of copolymers : $PC_{70}BM$. Different solvents (chlorobenzene (CB) and 1,2-dichlorobenzene (DCB)) were tested to build an optimized interpenetrated network in the active film, and the corresponding film properties and the photovoltaic device performance are discussed in detail.

2 Results and discussion

2.1 Material synthesis

To obtain the three designed copolymers a Stille reaction was employed as shown in Scheme 1. Subsequently, the three polymers PDTP-BT, PDTP-DTBT, and PDTP-DT2BT were synthesized by coupling of 2,6-di(trimethyltin)-*N*-[2′-ethylhexyl]-3-ethylheptanyla-dithieno[3,2-*b*:2′,3′-*d*]pyrrole (**1**) and 4,7-dibromo-2,1,3-benzothiadiazole (**M0**), 4,7-di(2′-bromothien-5′-yl)-2,1,3-benzothiadiazole (**M1**) and 4,7-di(2,2′-bromothien-5′-yl)-2,1,3-benzothiadiazole (**M2**) with tetrakis(triphenylphosphine)palladium(0) as a catalyst in yields of 55%, 65% and 82%, respectively. The chemical structures of these copolymers were verified by ^1H NMR spectroscopy. All of these copolymers are soluble in common organic solvents such as $CHCl_3$, CB and DCB due to the branched-chain substituent on the DTP moiety.

2.2 Optical properties

Fig. 1 shows the optical absorption spectra of PDTP-BT, PDTP-DTBT and PDTP-DT2BT in $CHCl_3$ solution and in thin films spin-coated on quartz plates. The absorption maximum wavelength in the solutions and the films and the optical band gap deduced from the absorption onsets are summarized in Table 1. Judging from the splitting of the absorption bands, it can be speculated that the polymers have the typical absorption characteristics of D–A type copolymers with π–π* and charge transfer-type transitions.

Comparing the polymers PDTP-BT and PDTP-DT2BT with the previously synthesized polymer PDTP-DTBT,[27] the difference in their absorption is distinct. The PDTP-DTBT solution showed two prominent absorption maxima at 450 and 671 nm, while PDTP-BT and PDTP-DT2BT solutions demonstrated two main absorption maxima at 413 and 711 nm and at 480 and 603 nm, respectively. Although the absorption peaks in the

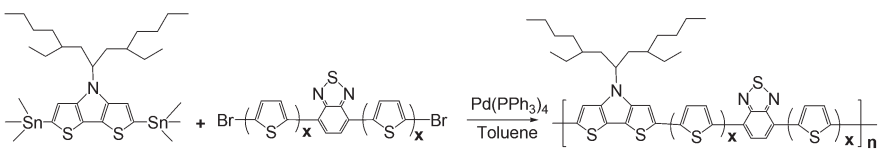

Scheme 1 Synthetic route of three dithienopyrrole-based donor–acceptor type copolymers with thienyl spacers.

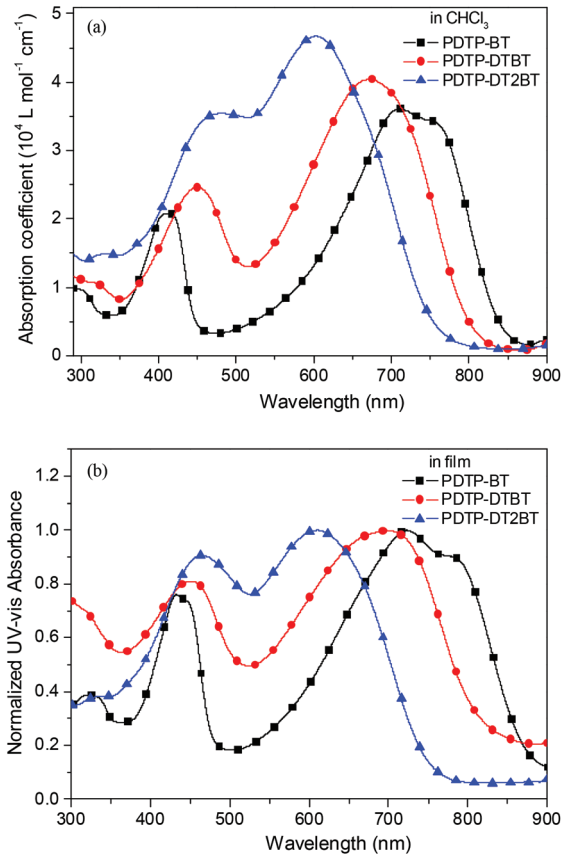

Fig. 1 UV-vis absorption spectra of the three polymers PDTP-BT, PDTP-DTBT and PDTP-DT2BT (a) in $CHCl_3$ solution and (b) in a film on a quartz plate.

long wavelength blue-shifted by 40 nm and 108 nm with insertion of one and two thienyl spacers to PDTP-BT, the absorption coefficients at the absorption maxima increase from 3.6×10^4 (PDTP-BT) to 4.0×10^4 (PDTP-DTBT) and 4.7×10^4 L mol^{-1} cm^{-1} (PDTP-DT2BT), respectively.

In thin films, the three copolymers exhibit similar shapes and red-shifted absorption spectra compared with those in the solutions, which indicates stronger intermolecular interactions in the solid state.[38] In addition, the PDTP-BT film shows a large shoulder peak at 800 nm, while no shoulder peaks were observed for PDTP-DTBT and PDTP-DT2BT, indicating stronger intermolecular interaction in PDTP-BT than in the others. These results suggest that on the absorption of the polymers, both absorption peaks and absorption coefficients could be readily controlled by tailoring the number of thienyl spacers along the polymers.[37,39,40]

The absorption edge shifts from *ca.* 900 nm in PDTP-BT to *ca.* 850 nm in PDTP-DTBT and *ca.* 750 nm in PDTP-DT2BT, reflecting the broadening of the optical band-gap in sequence. Table 1 shows the optical band-gaps (E_g^{opt}) of all polymers estimated from the corresponding UV-vis absorption onset. PDTP-DT2BT, PDTP-DTBT and PDTP-BT have optical band gaps of 1.61, 1.46 and 1.41 eV, respectively, which are close to the ideal value of 1.5 eV for PSC application.

These changes of the absorption spectra upon the introduction of thienyl groups can be qualitatively understood from density functional theory (DFT) calculations of the corresponding model compounds (Fig. S1†). The optimized structures show that all the polymer backbones are mostly planar. Time dependent DFT calculations show that the absorption band in the longer wavelength is mainly attributed to the transition from HOMO delocalized in the D–A backbone to LUMO localized in DTP units for all the polymers. On the other hand, the absorption in the shorter wavelength is largely contributed by the transition from HOMO to LUMO+1, which is similar to π–π^* transition in polythiophene judging by the shape of the orbitals. Therefore, the introduction of more thienyl spacer could stabilize LUMO+1 (π^*) due to the better conjugation, resulting in the red-shift of the absorption band. At the same time, it could decrease the D–A nature of the polymer due to the weaker electron acceptability of DTP, resulting in the blue-shift of the charge transfer bands.

2.3 Electrochemical properties

Electrochemical cyclic voltammetry has been widely employed to investigate the electrochemical behavior of the polymers and estimate the HOMO and the LUMO energy levels of the conjugated polymers. Representative cyclic voltammogram (CV) curves of these copolymers are shown in Fig. 2, while the obtained HOMO and LUMO values are summarized in Table 1. The onset reduction potential (φ_{red}) of PDTP-BT is −1.29 V *vs.* Fc/Fc$^+$, while the onset oxidation potential (φ_{ox}) is +0.18 V *vs.* Fc/Fc$^+$. From the values of reduction potential and oxidation potential, the LUMO and HOMO energy levels of PDTP-BT were calculated to be −3.51 and −4.98 eV, according to the equations LUMO = $-e(\varphi_{red} + 4.8)$ (eV) and HOMO = $-e(\varphi_{ox} + 4.8)$ (eV). The LUMO and HOMO energy levels of PDTP-DTBT and PDTP-DT2BT were estimated by a similar method to be

Table 1 The optical and electrochemical properties of three polymers

			UV-vis absorption spectra			Cyclic voltammetry		
			Solution	Film		p-doping	n-doping	
Polymers	M_w (kg mol^{-1})	PDI	λ_{max} (nm)	λ_{max} (nm)	E_g^{opt} (eV)	φ_{ox}/HOMO (V)/(eV)	φ_{red}/LUMO (V)/(eV)	E_g^{ec} (eV)
PDTP-BT	16.3	2.8	413/711	433/723	1.41	0.18/−4.98	−1.29/−3.51	1.47
PDTP-DTBT	6.0	3.4	450/671	451/697	1.46	0.20/−5.00	−1.37/−3.43	1.57
PDTP-DT2BT	21.2	2.3	480/603	464/611	1.61	0.19/−4.99	−1.40/−3.40	1.60

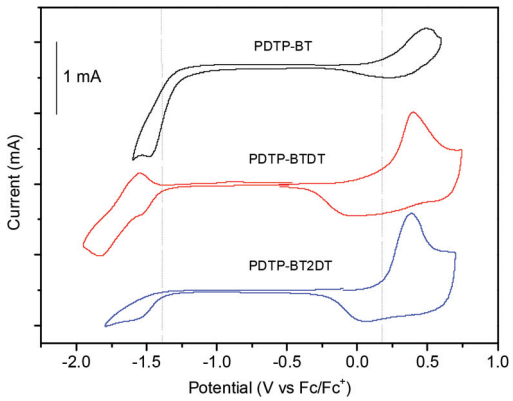

Fig. 2 Cyclic voltammograms of the polymer films deposited on a platinum plate (~1 cm^2) in an acetonitrile solution of 0.1 M $[Bu_4N]PF_6$ (Bu = butyl) at a scan rate of 50 mV s^{-1}.

−3.43, −3.40 eV and −5.00, −4.99 eV, respectively. These results indicate that changing the number of thienyl spacers along the conjugated copolymers has an obvious effect on the LUMO energy level. The electrochemical band-gaps (E_g^{EC}) of all polymers are in accordance with the results of E_g^{opt}.

2.4 Microstructure

Crystalline order of the copolymer thin films was investigated by X-ray diffraction (XRD) scans (Fig. S2†). In the out-of-plane measurement, the XRD pattern of PDTP-BT reveals a weak peak near 6°, and there is no clear peak for PDTP-DTBT and PDTP-DT2BT, suggesting that they exhibit amorphous structures in the film, which might be due to the bulky side chain in the DTP building block. A change in the number of thienyl spacers in this system does not significantly affect the aggregation behaviour of the polymer main chains.

The microstructure of blend films of the copolymers with fullerene derivatives is known to have a large effect on the charge transport properties and the corresponding efficiencies of PSCs. Here, the atomic force microscopy (AFM) was applied to investigate the morphology of the blend film of the polymer : $PC_{70}BM$ fabricated from CB and DCB solutions, respectively, as shown in Fig. 3. For PDTP-BT : $PC_{70}BM$, both CB and DCB gave the films with obvious phase separation with a root mean square (RMS) of 2.222 nm and 0.880 nm, respectively, which might be due to the poor miscibility of the two materials. For PDTP-DTBT and PDTP-DT2BT, the blend film of polymer/$PC_{70}BM$ spin-coated from CB was also rough, but the blend films fabricated from DCB displayed a much smoother surface with a RMS of 0.188 nm and 0.259 nm, respectively. This smaller roughness of the blend film indicates that the domain size of the phase separation of the donor–acceptor interpenetrating network could be reduced, which could be beneficial for the exciton charge separation and charge transport. These results indicate that the morphologies of these polymers with $PC_{70}BM$ are quite sensitive to the solvents used for device processing and the introduction of a thienyl spacer could improve the miscibility.

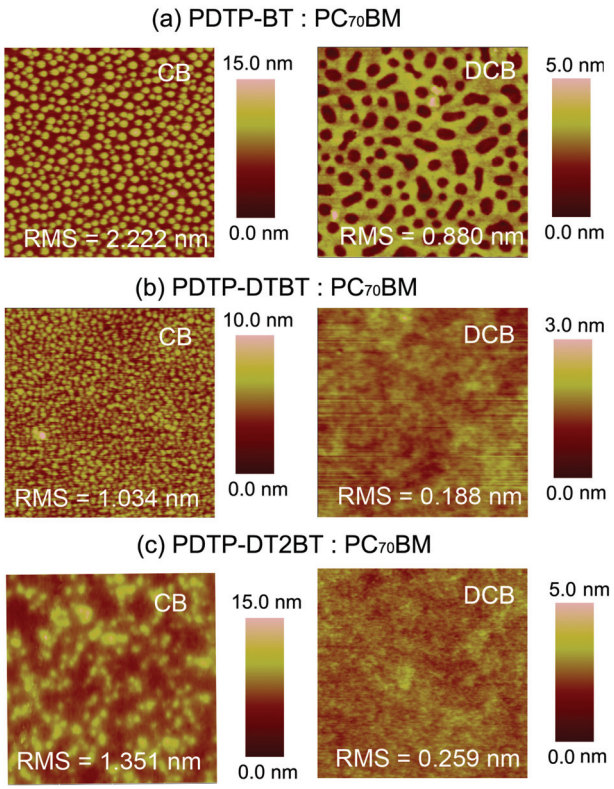

Fig. 3 AFM height images of the mixed films with $PC_{70}BM$ and (a) PDTP-BT, (b) PDTP-DTBT and (c) PDT-DT2BT spin-coated from different solutions (CB and DCB) (image size: 4 μm × 4 μm).

2.5 Photovoltaic properties

The photovoltaic properties of the three copolymers PDTP-BT, PDTP-DTBT and PDTP-DT2BT were studied by fabricating bulk heterojunction BHJ-type PSCs with a conventional sandwich configuration of ITO/PEDOT : PSS/polymer : $PC_{70}BM$/Ca/Al. The effective areas of the PSCs, contributing to photocurrent, were defined using a metal photomask during irradiation with simulated solar light. The devices were optimized by changing many factors, such as the ratio of the donor and the acceptor, the thickness of blend films and the cathode metal. The best performance was obtained with the thickness of the active layer of 80–90 nm, the copolymers : $PC_{70}BM$ ratio of 1 : 2 (by weight) and the Ca/Al used as the cathode.

Fig. 4 shows the *J*–*V* curves of the optimized PSCs based on the three polymers under illumination of AM 1.5 simulated solar light (100 mW cm^{-2}). The PSCs with two kinds of solvents CB and DCB for the spin-coating of the active layers were investigated, and the corresponding photovoltaic parameters of the devices open-circuit voltage (V_{OC}), short-circuit current density (J_{SC}), fill factor (FF) and PCE are summarized in Table 2. When CB was used as the solvent, all the combinations showed a relatively low PCE of 0.87%, 1.97% and 1.92% in the devices with PDTP-BT : $PC_{70}BM$, PDTP-DTBT : $PC_{70}BM$ and PDTP-DT2BT : $PC_{70}BM$ respectively. The DCB solvent induced high performance photovoltaic devices due to the optimized interpenetrated network of the active film. The

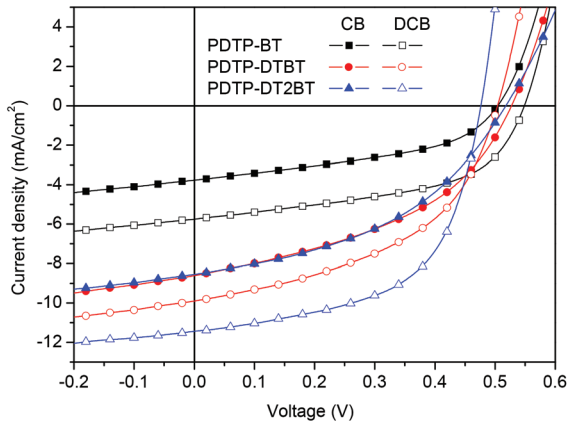

Fig. 4 *J–V* curves of the polymer solar cells based on PDTP-BT, PDTP-DTBT and PDTP-DT2BT under the illumination of AM 1.5, 100 mW cm^{-2}.

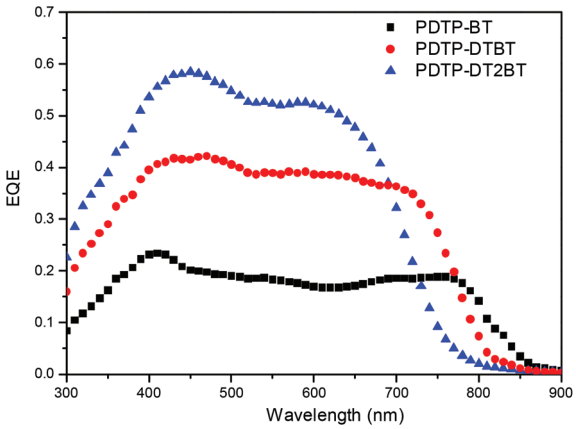

Fig. 5 EQE curves of the polymer solar cells based on PDTP-BT, PDTP-DTBT and PDTP-DT2BT under the illumination of AM 1.5, 100 mW cm^{-2}.

Table 2 Device characteristics of PSCs based on the DTP and BT based copolymers in combination with $PC_{70}BM$

Polymer : acceptor (wt/wt)	Solvent	V_{OC} (V)	J_{SC} (mA cm^{-2})	FF	PCE
PDTP-BT : $PC_{70}BM$ (1 : 2)	CB	0.50	3.77	0.45	0.87%
	DCB	0.54	5.75	0.53	1.64%
PDTP-DTBT : $PC_{70}BM$ (1 : 2)	CB	0.52	8.61	0.44	1.97%
	DCB	0.50	9.90	0.48	2.37%
PDTP-DT2BT : $PC_{70}BM$ (1 : 2)	CB	0.52	8.55	0.43	1.92%
	DCB	0.48	11.43	0.57	3.12%

best devices of PDTP-BT and PDTP-DTBT show PCE of 1.64% and 2.37%, respectively. The polymer PDTP-DT2BT exhibits the highest PCE of 3.12%, ascribed to the largest J_{SC} = 11.43 mA cm^{-2} with a slightly lower V_{OC} of 0.54 V and a slightly higher FF of 0.57 than the other polymers. The V_{OC} values of the devices are around 0.5 V, suggesting that the addition of the thienyl units does not affect the main chain distortion. This coincides well with similar HOMO energy levels for the copolymers measured by CV. These results indicate that the PCEs of the photovoltaic devices based on PDTP-DT2BT : $PC_{70}BM$ were higher than those of PDTP-DTBT : $PC_{70}BM$ and PDTP-BT : $PC_{70}BM$. Overall, it is an effective approach to improve the photovoltaic performance of PDTP-based copolymers by increasing the number of unsubstituted thienyl units along the copolymers backbone.

Fig. 5 shows the external quantum efficiency (EQE) plots of the devices based on three copolymer : $PC_{70}BM$ combinations under the illumination of monochromatic light. With the increase of thienyl spacers, the EQE response wavelengths show a blue shift, a similar tendency to the absorption spectra, but the EQE peak values were higher in PDTP-DT2BT (58%) compared to PDTP-BT (23%) or PDTP-DTBT (42%). The shapes of the EQE curves of the devices in the range of 450–700 nm could be assigned to the stronger absorption of $PC_{70}BM$.

3 Conclusions

In conclusion, three low band gap D–A copolymers, based on the DTP donor and the BT acceptor, with different numbers of thienyl spacers along the backbone have been designed and synthesized. The thienyl spacer makes the absorption spectra peak blue-shift in the longer wavelength range and red-shift in the low wavelength range. Under 1.5 G 100 mW cm^{-2} illumination, a best PCE of 3.12% for PDTP-DT2BT was recorded, with V_{OC} = 0.48 V, J_{SC} = 11.43 mA cm^{-2}, and FF = 0.57. Although the best PCE is still not high enough for commercial use, our optimization by designing suitable molecular structures, selecting different solvents and changing other factors could provide useful information for further studies of the commercialized PSCs.

4 Experimental section

4.1 Materials

All the chemicals were purchased from Alfa, Aldrich or Wako and were used without further purification. The following compounds were synthesized according to the procedure in the literature: 2,6-di(trimethyltin)-*N*-[2′-ethylhexyl]-3-ethylheptanyla-dithieno[3,2-*b*:2′,3′-*d*]pyrrole (**1**) and 4,7-di(2,2′-bithien-5-yl)-2,1,3-benzothiadiazole (**M2**).[27]

4.2 Synthesis of polymers

The three polymers were synthesized by a similar procedure to the synthesis of PDTP-DTBT (M_w = 6.0 kg mol^{-1}; polydispersity index (PDI) = 3.4) in our previous report.[27] For PDTP-BT, the detailed synthetic process is as follows: **1** (0.56 mmol, 416 mg), **M0** (0.56 mmol, 165 mg), and dry toluene (15 mL) were added to a 50 mL double-neck round bottom flask. The reaction container was purged with N_2 for 30 min to remove O_2. $Pd(PPh_3)_4$ (5%, 32 mg) was added and heated up to 110 °C. The solution was stirred at 110 °C for 48 h. The dark blue sticky solution

was cooled down to room temperature and poured into methanol (200 mL), and the dark green precipitates were collected by filtration and then washed with methanol. The solid was dissolved in $CHCl_3$ (150 mL) and passed through a column packed with alumina, Celite, and silica gel. The column was eluted with $CHCl_3$. The combined polymer solution was concentrated to 30 mL and was poured into methanol (300 mL). After this, the precipitates were collected and dried (170 mg, 55%). ^{1}H NMR ($CDCl_3$, 400 MHz): δ (ppm): 8.0–7.1 (m, 4H), 4.5 (br, 1H), 2.1–0.5 (m, 34H). M_w = 16.3 kg mol^{-1}; PDI = 2.80.

A similar synthetic route for PDTP-DT2BT is also shown in Scheme 1, starting with **1** (0.53 mmol, 394 mg), **M2** (0.53 mmol, 330 mg), dry toluene (15 mL) and $Pd(PPh_3)_4$ (5%, 31 mg). Yield: 380 mg (82%). ^{1}H NMR ($CDCl_3$, 400 MHz): δ(ppm): 8.0–6.1 (m, 4H), 4.4 (br, 1H), 2.0–0.6 (m, 34H). M_w = 21.2 kg mol^{-1}; PDI = 2.30.

4.3 Characterization

^{1}H NMR (400 MHz) spectra were measured using a JEOL Alpha FT-NMR spectrometer equipped with an Oxford superconducting magnet system at 400 MHz in deuterated chloroform solution with TMS as a reference. Gel permeation chromatography (GPC) was performed on a Shimadzu Prominence system equipped with a UV detector using $CHCl_3$ containing triethylamine as the eluent. Absorption spectra were measured using a SHIMADZU spectrophotometer MPC-3100. Cyclic voltammograms (CVs) were recorded on an HSV-100 (Hokuto Denkou) potentiostat. A Pt plate coated with a thin polymer film was used as the working electrode. A Pt wire and an Ag/Ag+ (0.01 M of $AgNO_3$ in acetonitrile) electrode were used as the counter and the reference electrodes (calibrated *vs.* Fc/Fc^+), respectively. AFM measurement was carried out using a Digital Instrumental Nanoscope 31 operated in the tapping mode. Out-of-plane and in-plane XRD scans of polymer thin films on silicon wafer substrates were performed on a Smartlab X-ray diffractometer (Rigaku) using monochromatized Cu Kα radiation (λ = 0.154 nm) generated at 45 kV and 200 mA.

4.4 Fabrication and characterization of polymer solar cells

PSCs were constructed in the traditional sandwich structure through several steps. ITO-coated glass substrates were cleaned by ultrasonication sequentially in detergent, water, acetone, and 2-propanol. After drying the substrate, PEDOT : PSS (Baytron P) was spin-coated (4000 rpm for 30 s) on ITO. The film was dried at 140 °C under a N_2 atmosphere for 30 min. After cooling the substrate, a chlorobenzene solution of the PDTP-DTBT and $PC_{70}BM$ mixture (1 : 2, by weight) was spin-coated. The PDTP-DTBT concentration was 10 mg mL^{-1}. Ca and Al electrodes were then successively evaporated under high vacuum (approximately 2 × 10^{-4} Pa) in the ULVAC UPC-260F vacuum evaporation system. The thickness of the Ca electrode was 20 nm, and that of the Al electrode was 60 nm. The current–voltage characteristics of the solar cells were measured using the Agilent Technologies E5273A C-V measurement system. PCE was examined using a xenon-lamp-based solar simulator (Peccell Technologies PCE-L11). Light intensity was adjusted using a standard silicon solar cell with an optical filter (Bunkou Keiki BS520).

Acknowledgements

We acknowledge financial support from the New Energy and Industrial Technology Development Organization (NEDO), Japan. We also acknowledge the support from the National Natural Science Foundation (Nos. 51203030, 51473040).

Notes and references

1 C. J. Brabec, N. S. Sariciftci and J. C. Hummelen, *Adv. Funct. Mater.*, 2001, **11**, 15–26.
2 D. Mühlbacher, M. Scharber, M. Morana, Z. Zhu, D. Waller, R. Gaudiana and C. Brabec, *Adv. Mater.*, 2006, **18**, 2884–2889.
3 K. M. Coakley and M. D. McGehee, *Chem. Mater.*, 2004, **16**, 4533–4542.
4 G. Yu, J. Gao, J. C. Hummelen, F. Wudl and A. J. Heeger, *Science*, 1995, **270**, 1789–1791.
5 S. E. Shaheen, C. J. Brabec, N. S. Sariciftci, F. Padinger, T. Fromherz and J. C. Hummelen, *Appl. Phys. Lett.*, 2001, **78**, 841–843.
6 P. W. M. Blom, V. D. Mihailetchi, L. J. A. Koster and D. E. Markov, *Adv. Mater.*, 2007, **19**, 1551–1566.
7 J. G. Labram, J. Kirkpatrick, D. D. C. Bradley and T. D. Anthopoulos, *Adv. Energy Mater.*, 2011, **1**, 1176–1183.
8 M. C. Scharber, D. Mühlbacher, M. Koppe, P. Denk, C. Waldauf, A. J. Heeger and C. J. Brabec, *Adv. Mater.*, 2006, **18**, 789–794.
9 J. Hou, Z. A. Tan, Y. Yan, Y. He, C. Yang and Y. Li, *J. Am. Chem. Soc.*, 2006, **128**, 4911–4916.
10 Y. Li and Y. Zou, *Adv. Mater.*, 2008, **20**, 2952–2958.
11 Y. Liang, D. Feng, Y. Wu, S. T. Tsai, G. Li, C. Ray and L. Yu, *J. Am. Chem. Soc.*, 2009, **131**, 7792–7799.
12 J. Hou, H. Y. Chen, S. Zhang, G. Li and Y. Yang, *J. Am. Chem. Soc.*, 2008, **130**, 16144–16145.
13 H. Y. Chen, J. Hou, S. Zhang, Y. Liang, G. Yang, Y. Yang, L. Yu, Y. Wu and G. Li, *Nat. Photonics*, 2009, **3**, 649–653.
14 M. Svensson, F. Zhang, S. C. Veenstra, W. J. H. Verhees, J. C. Hummelen, J. M. Kroon, O. Inganäs and M. R. Andersson, *Adv. Mater.*, 2003, **15**, 988–991.
15 J. Peet, J. Y. Kim, N. E. Coates, W. L. Ma, D. Moses, A. J. Heeger and G. C. Bazan, *Nat. Mater.*, 2007, **6**, 497–500.
16 J. C. Bijleveld, M. Shahid, J. Gilot, M. M. Wienk and R. A. J. Janssen, *Adv. Funct. Mater.*, 2009, **19**, 3262–3270.
17 Z. Li, S. W. Tsang, X. M. Du, L. Scoles, G. Robertson, Y. G. Zhang, F. Toll, Y. Tao, J. P. Lu and J. F. Ding, *Adv. Funct. Mater.*, 2011, **21**, 3331–3336.
18 Y. J. Cheng, Y. J. Ho, C. H. Chen, W. S. Kao, C. E. Wu, S. L. Hsu and C. S. Hsu, *Macromolecules*, 2012, **45**, 2690–2698.

19 S. Das, P. B. Pati and S. S. Zade, *Macromolecules*, 2012, **45**, 5410–5417.
20 C. Y. Chang, L. Zuo, H. L. Yip, Y. Li, C. Z. Li, C. S. Hsu, Y. J. Cheng, H. Chen and A. K. Y. Jen, *Adv. Funct. Mater.*, 2013, **23**, 5084–5090.
21 M. C. Scharber, M. Koppe, J. Gao, F. Cordella, M. A. Loi, P. Denk, M. Morana, H. J. Egelhaaf, K. Forberich, G. Dennler, R. Gaudiana, D. Waller, Z. Zhu, X. Shi and C. J. Brabec, *Adv. Mater.*, 2010, **22**, 367–370.
22 H. Y. Chen, J. Hou, A. E. Hayden, H. Yang, K. N. Houk and Y. Yang, *Adv. Mater.*, 2010, **22**, 371–375.
23 T. Y. Chu, J. Lu, S. Beaupré, Y. Zhang, J. R. Pouliot, S. Wakim, J. Zhou, M. Leclerc, Z. Li, J. Ding and Y. Tao, *J. Am. Chem. Soc.*, 2011, **133**, 4250–4253.
24 C. M. Amb, S. Chen, K. R. Graham, J. Subbiah, C. E. Small, F. So and J. R. Reynolds, *J. Am. Chem. Soc.*, 2011, **133**, 10062–10065.
25 Z. P. Fei, J. S. Kim, J. Smith, E. B. Domingo, T. D. Anthopoulos, N. Stingelin, S. E. Watkins, J. S. Kim and M. Heeney, *J. Mater. Chem.*, 2011, **21**, 16257–16263.
26 J. Y. Liu, R. Zhang, G. Sauve, T. Kowalewski and R. D. McCullough, *J. Am. Chem. Soc.*, 2008, **130**, 13167–13176.
27 E. Zhou, M. Nakamura, T. Nishizawa, Y. Zhang, Q. Wei, K. Tajima, C. Yang and K. Hashimoto, *Macromolecules*, 2008, **41**, 8302–8305.
28 E. Zhou, S. Yamakawa, K. Tajima, C. Yang and K. Hashimoto, *Chem. Mater.*, 2009, **21**, 4055–4061.
29 E. Zhou, J. Cong, K. Hashimoto and K. Tajima, *Energy Environ. Sci.*, 2012, **5**, 9756–9759.
30 H. Zhou, L. Yang, S. C. Price, K. J. Knight and W. You, *Angew. Chem., Int. Ed.*, 2010, **49**, 7992–7995.
31 K. H. Ong, S. L. Lim, H. S. Tan, H. K. Wong, J. Li, Z. Ma, L. C. H. Moh, S. H. Lim, J. C. de Mello and Z. K. Chen, *Adv. Mater.*, 2011, **23**, 1409–1413.
32 L. H. Slooff, S. C. Veenstra, J. M. Kroon, D. J. D. Moet, J. Sweelssen and M. M. Koetse, *Appl. Phys. Lett.*, 2007, **90**, 143506.
33 P. L. T. Boudreault, A. Michaud and M. Leclerc, *Macromol. Rapid Commun.*, 2007, **28**, 2176–2179.
34 E. Wang, L. Wang, L. Lan, C. Luo, W. Zhuang, J. Peng and Y. Cao, *Appl. Phys. Lett.*, 2008, **92**, 033307.
35 N. Blouin, A. Michaud and M. Leclerc, *Adv. Mater.*, 2007, **19**, 2295–2300.
36 L. Liao, L. Dai, A. Smith, M. Durstock, J. Lu, J. Ding and Y. Tao, *Macromolecules*, 2007, **40**, 9406–9412.
37 M. Zhang, X. Guo, Z. G. Zhang and Y. Li, *Polymer*, 2011, **52**, 5464–5470.
38 G. Li, V. Shrotriya, J. Huang, Y. Yao, T. Moriarty, K. Emery and Y. Yang, *Nat. Mater.*, 2005, **4**, 864–868.
39 M. J. Zhang, X. Guo and Y. F. Li, *Macromolecules*, 2011, **44**, 8798–8804.
40 P. M. Beaujuge, W. Pisula, H. N. Tsao, S. Ellinger, K. Müllen and J. R. Reynolds, *J. Am. Chem. Soc.*, 2009, **131**, 7514–7515.